PNAS RESEARCH ARTICLE | DEVELOPMENTAL BIOLOGY OPEN ACCESS

Dmrt2 and Hmx2 direct intercalated cell diversity in the mammalian kidney through antagonistic and supporting regulatory processes

Riana K. Parvez[a,1], Doh Kyung Kim[a], Réka L. Csipán[a], Jinjin Guo[a], Zipeng Zeng[a,b], Chennan C. Zhang[a,b], Zhongwei Li[a,b], and Andrew P. McMahon[a,2,3]

Edited by Martin Pollak, Beth Israel Deaconess Medical Center, Brookline, MA; received September 10, 2024; accepted January 15, 2025

Intercalated cells (ICs) in the mammalian kidney regulate circulatory pH through IC subtype–restricted actions of bicarbonate transporters: pH is elevated by Slc4a1 restricted to type A-ICs (A-ICs) and depressed by Slc26a4 in type B-IC (B-ICs). NonA-nonB-ICs (nA/nB-ICs) also produce Slc26a4 though their function is unclear. Though both nephron and ureteric progenitor lineages generate A-ICs, the former also generates nA/nB-ICs and the latter B-ICs. Lineage and cell type restricted transporter gene expression in the mouse and human kidney is preceded by expression of the transcriptional regulators *Dmrt2/DMRT2* in A-ICs, and either, or both, *Hmx2/HMX2* and *Hmx3/HMX3* in B- and nA/nB ICs. CRISPR/Cas9-directed removal of *Dmrt2* and the linked *Hmx2/Hmx3 genes* resulted in IC-subtype switching. A-ICs adopted an *Hmx2*$^+$/*Slc26a4*$^+$ B-IC cell fate on Dmrt2 removal while B-ICs initiated a Dmrt2$^+$/Slc4a1$^+$ A-IC program on *Hmx2/Hmx3* removal. Triple knockout of *Dmrt2*, *Hmx2*, and *Hmx3* resulted in hybrid ICs expressing both *Slc4a1* and *Slc26a4*. Thus, restricted expression of these regulators is essential for specifying IC subtypes. To explore these mechanisms, *Hmx2* and *Dmrt2* were activated ectopically in ureteric organoid cultures. Introduction of *Foxi1*—a pan determinant of ICs—activated early *Dmrt2*$^+$ A-IC development while cointroduction of *Hmx2* silenced Foxi1-dependent *Dmrt2* expression and led to an upregulation of Slc26a4. In contrast, coexpression of *Foxi1* and *Dmrt2* upregulated *Slc4a1*. These data support a model in which mutually repressive interactions between *Dmrt2* and *Hmx2/3* establish distinct IC identities and ongoing activity of these factors supports gene regulatory programs specific to each IC subtype.

kidney | development | collecting duct

Significance

Subtypes of intercalated cells in the mammalian kidney arise from multiple lineages and regulate circulatory pH homeostasis through opposing actions on ion transport. Subtype diversity correlates with mutually exclusive expression of the transcriptional regulators *Dmrt2* and *Hmx2/Hmx3*. Subtype-enriched activity of these transcription factors is shown to drive IC diversity, an insight that will inform approaches to engineer functional kidney surrogates.

In the adult mammalian kidney, principal cells (PCs) and intercalated cells (ICs) work together to regulate water, salt, and pH homeostasis (1). In the control of pH balance, discrete IC subtypes perform opposing functions to either secrete acid or bicarbonate into the lumen for excretion in the urine. Three subtypes of ICs develop within the adult mammalian kidney: type A (A-IC), type B (B-IC), or non-A/non-B (nA/nB-IC). ICs are formed from two distinct cell lineages during the course of kidney development and occupy distinct spatial positions within the kidney (2–11). Nephron progenitor cell (NPC) derivatives generate nAnB-ICs and A-ICs within the cortically restricted connecting segment (2, 12). The connecting segment transitions into the ureteric progenitor cell (UPC)-derived collecting duct epithelium. In the kidney cortex, this epithelium generates A- and B-IC subtypes, whereas only A-IC subtypes are present in medullary collecting epithelium (3–11).

The importance of IC cell functions is highlighted by mutational analysis. Failure to develop ICs leads to distal renal tubular acidosis (dRTA) which affects body systems beyond the kidney (13–15). IC subtypes are distinguished by distinct gene expression programs (1). Microdissection and single-cell profiling of the adult mouse and human kidney have identified cohorts of genes expressed specifically in ICs, some of which, like the bicarbonate transporters Slc4a1/AE1 and Slc26a4/Pendrin, show subtype-specific gene expression (12, 16, 17). In the human kidney, loss of SLC4A1 results in dRTA (18–20). Loss of SLC26A4 activity leads to Pendred syndrome characterized by deafness, reflecting SLC26A4 actions in sensory hair cells, and metabolic alkalosis upon bicarbonate challenge, reflecting disrupted B-IC functions in the kidney (21–25).

Mouse genetic studies have provided insight into an emerging transcriptional hierarchy specifying ICs. *Tfcp2l1* and *Foxp1* are both broadly expressed in PC and IC progenitors but only required for IC specification, and *Foxi1* acts downstream of Tfcp2l1 specifically within the IC lineage to initiate IC development (13, 26, 27). Notch signaling has been shown to restrict IC cell specification. Notch ligands are expressed by ICs and Notch signaling inhibits adjacent epithelial cells from adopting an IC fate, thereby promoting

Author affiliations: [a]Department of Stem Cell and Regenerative Medicine, University of Southern California, Los Angeles, CA 90033; and [b]University of Southern California/University Kidney Research Organization Kidney Research Center, Division of Nephrology and Hypertension, Department of Medicine, Keck School of Medicine, University of Southern California, Los Angeles, CA 90033

Author contributions: R.K.P., D.K.K., and A.P.M. designed research; R.K.P., D.K.K., R.L.C., and J.G. performed research; Z.Z., C.C.Z., and Z.L. contributed new reagents/analytic tools; R.K.P., D.K.K., R.L.C., and A.P.M. analyzed data; R.K.P., D.K.K, and A.P.M. conceptualized the experiments; R.K.P., D.K.K, and A.P.M. analyzed the experiments; R.K.P., D.K.K, R.L.C., and J.J.G. collected data; and R.K.P., D.K.K., and A.P.M. wrote the paper.

The authors declare no competing interest.

This article is a PNAS Direct Submission.

[1]Present address: Renasant Bio, Berkeley, CA 94720.

[2]Present address: Division of Biology and Biological Engineering, California Institute of Technology, Pasadena, CA 91125.

[3]To whom correspondence may be addressed. Email: amcmahon@caltech.edu.

This article contains supporting information online at https://www.pnas.org/lookup/suppl/doi:10.1073/pnas.2418471122/-/DCSupplemental.

Published May 12, 2025.

PC fates (27–30). How Notch signaling interfaces with PC and IC specifying transcriptional programs is unclear. At the subtype level, several studies have distinguished IC subtype–restricted programs of gene expression in the adult mouse and human kidney, including subtype-specific expression of genes encoding the transcriptional regulators Dmrt2 in A-ICs, Hmx2 in nA/nB-ICs, and Hmx2 and Hmx3 in B-ICs (12, 16, 17). Recent mutational studies support a role for *Dmrt2* in specification of the A-IC fate (26).

In this study, we applied loss-of-function analyses of the mouse kidney in vivo, and gain-of-function approaches in an organoid model in vitro, to investigate the developmental actions of *Dmrt2*, and *Hmrt2* and *Hmx3* (*Hmx2/3*) in IC lineages. These studies demonstrate Dmrt2 and Hmx2/Hmx3 direct alternative IC fate choices through a mutual inhibitory mechanism and highlight lineage- and position-associated variability within IC subtype programs.

Results

Early *DMRT2* and *HMX2* Expression Distinguishes Mammalian IC Subtypes. Examination of adult mouse (12) and human kidney (17) single-cell transcriptional profiling documented expressions of *Doublesex and mab3 related transcription factor 2* (*Dmrt2*/*DMRT2*) and *H6 Family Homeobox 2 and 3 members* (*Hmx2*/*HMX2 and Hmx3*/*HMX3*) specific to mature adult A-IC, and B- and nA/nB-IC subtypes, respectively (Fig. 1*A* and *SI Appendix*, Fig. S1*A*). Analysis of UPC-derived *Foxi1*$^+$/*Foxp1*$^+$ IC subtypes at the onset of IC specification in the postnatal day (P)0 mouse kidney (31) (Fig. 1*B* and *SI Appendix*, Fig. S1*B*) identified mutually exclusive *Dmrt2*$^+$/*Slc4a1*$^+$ and *Hmx2*$^+$/*Slc26a4*$^+$ clusters indicative of early A-IC and B-IC development (Fig. 1*B* and *SI Appendix*, Fig. S1*C*). A similar analysis of single nuclear multiomic data from an 18-wk fetal kidney sample also identified *FOXI1*$^+$/*FOXP1*$^+$ IC clusters distinguished by mutually exclusive expression of *SLC4A1*/*DMRT2* and *SLC26A4*/*HMX2*/*HMX3* (Fig. 1*C* and *SI Appendix*, Fig. S1*D*). Whereas *Dmrt2* displays A-IC subtype restricted expression in both NPC and UPC lineages, NPC-derived nA/nB-ICs express *Hmx2* exclusively, and UPC-derived B-ICs express both *Hmx2* and *Hmx3* (Fig. 1 *B* and *C* and *SI Appendix*, Fig. S1*C*).

Monocle analysis highlighted the onset of expression of *Dmrt2*, *Hmx2,* and *Hmx3* after the activation of general IC determinants (*Tfcp2l1, Foxp1, and Foxi1),* and prior to the initiation of *Slc4a1* and *Slc26a4* expression consistent with *Dmrt2*, *Hmx2,* and *Hmx3* initiating IC subtype diversity (Fig. 1*D*). Consistent with these findings, RNAscope in situ hybridization highlighted mutually exclusive *Dmrt2* and *Hmx2* expression in the embryonic day (e)18.5 mouse kidney (32) (Fig. 1*E*). Distinguishing NPC and UPC derivatives utilizing a genetic lineage reporter (NPC-derivatives tdTomato$^+$ and UPC-derivatives tdTomato$^-$) demonstrated most *Hmx2*$^+$ cells within the NPC lineage and only rare *Hmx2*$^+$/*Hmx3*$^+$ B-ICs within the UPC lineage (Fig. 1*F*). Rare coexpression of *HMX2 and HMX3* was also observed in the fetal and adult human kidney transcriptomic datasets (Fig. 1*C* and *SI Appendix*, Fig. S1*A*). Within the developing mouse kidney, *Slc4a1* and *Dmrt2* have been detected during embryonic development in A-IC of the ureteric-derived collecting duct and the nephron-derived connecting tubule (32, 33). In the 18-wk human fetal kidney, *DMRT2* and *SLC4A1* expression colocalized to *FOXI1*$^+$ medullary localized A-ICs (Fig. 1*G*). In the cortex, *SLC26A4* expression was observed in conjunction with *FOXI1* and *HMX2* (Fig. 1*H*). The epithelial morphology suggests these are ureteric epithelial B-ICs. Not all *HMX2*-expressing cells showed *SLC26A4* coexpression, consistent with an earlier onset of gene expression directing cell fate to genes encoding mature IC cell type functions (Fig. 1*I*).

In summary, single-cell RNA-seq profiling and in vivo expression analysis indicate that *Dmrt2/DMRT2*, *Hmx2/HMX2,* and *Hmx3/HMX3* demarcate distinct IC subtypes shortly after the onset of IC cell programming in the developing mammalian kidney, which is maintained into the adult kidney.

Genetic Analysis of IC Subtype Specification. To examine the roles of Dmrt2 and Hmx2/Hmx3, we generated loss-of-function alleles through CRISPR/Cas9 gene editing. *Dmrt2* knockout (KO) targeted the 5′ end of the *Dmrt2* gene body generating a mutant allele with two separate deletions. In contrast to the 562aa Dmrt2 protein, an out-of-frame translation of the mutated transcript is predicted to generate a nonhomologous 164 amino acid (aa) protein (Fig. 2*A*). *Hmx2* and *Hmx3,* which have overlapping functions in specific developmental contexts (34–36), are separated by 15 kb in the mouse genome. Considering the potential for overlapping functions, we generated mutations removing both genes deleting the entire coding region for *Hmx3*, and all but a short 3′ region of *Hmx2* beyond the predicted DNA binding domain (Fig. 2*A*). Translation of the mutant allele predicts a nonhomologous 110aa protein product (Fig. 2*A*). Mice homozygous for the *Dmrt2* mutation (*Dmrt2* KO) die at birth from previously reported skeletal deficiencies (21). Though others have reported *Hmx2/Hmx3* KO mice survive to P10-P11 (35), in our hands all *Hmx2/Hmx3* KO died by P2. Consequently, we focused on the potential of these transcriptional regulators to initiate IC diversity at the onset of IC development.

Both *Dmrt2* KO and *Hmx2/Hmx3* KO kidneys were superficially normal on collection at e18.5. Bulk mRNA-seq on kidneys identified differential expressed genes (DEGs) between wild-type and *Dmrt2* KO, *Hmx2/Hmx3* KO, or *Dmrt2/Hmx2/Hmx3* KO kidneys (*Dmrt2* KO, n = 3; *Hmx2/Hmx3* KO, n = 6; *Dmrt2/Hmx2/Hmx3* KO, n = 3; $-0.25 \leq \log2\text{FoldChange} \geq 0.25$; adjusted *P*-value ≤ 0.05) (Dataset S1). On loss of *Dmrt2,* 173 genes were significantly down-regulated, while 161 were significantly up-regulated. No expression change was observed in genes broadly expressed in both A-IC and B-IC types such as *Foxi1*, *Foxp1,* and *Atp6v1b* family members associated with proton pumps operating in all IC cells (Fig. 2*B* and Dataset S1). In contrast, *Dmrt2* mutant kidneys showed a marked downregulation in the expression of *Dmrt2*, and a number of A-IC enriched genes including *Slc4a1, Aqp6, P2ry14, and Kit;* and, a corresponding upregulation in B- and/or nA/nB-IC enriched genes including *Hmx2*, *Slc26a4, Insrr,* and *Tldc2* (Fig. 2*B*, *SI Appendix*, Fig. S2 *A* and *B*, and Dataset S1). Thus, loss of *Dmrt2* did not impact specification of an IC fate. In contrast, the data are consistent with Dmrt2 promoting an A-IC fate, at least in part by suppressing an alternative B and/or nA/nB-IC IC fate. Further, enhanced expression of *Hmx2* in *Dmrt2* mutants indicates *Dmrt2* is required to repress *Hmx2*. Collectively, these findings at the onset of IC development are consistent with analyses of established IC types following conditional removal of *Dmrt2* 4 wk after birth (26).

Examining *Hmx2/Hmx3* KO kidneys at e18.5 identified few DEGs within the same cutoff threshold reflecting the small percentage of B- and nA/nB ICs in the kidney prior to birth (Fig. 2*C* and Dataset S2). In addition to the expected loss of *Hmx2* expression (*Hmx3* is normally expressed weakly below the cut-off), *Slc26a4* was significantly downregulated and *Dmrt2* significantly upregulated (Fig. 2*C* and Dataset S2). Further, just outside the cutoffs, among the top four up-regulated genes ranked by adjusted *P*-values were *Slc4a1* and *Oxgr1*, which show A-IC-specific

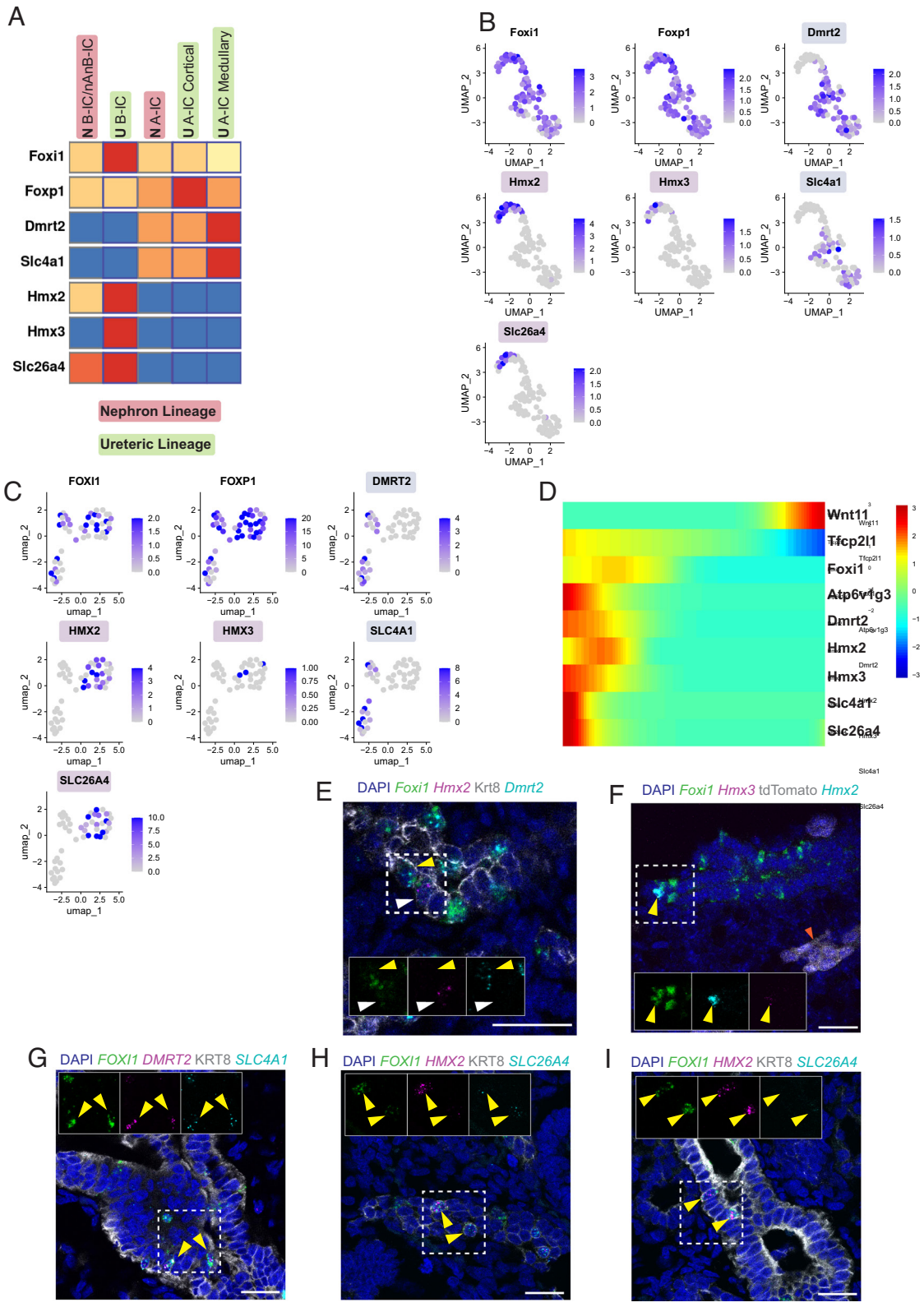

Fig. 1. Dmrt2 and Hmx2 have mutually exclusive expression within IC subtypes. (*A*) Expression of IC markers in the adult mouse kidney (12). (*B*) Feature plot of P0 mouse IC scRNAseq data for IC markers. (*C*) Expression of IC subtype markers in human fetal week 18 kidney. (*D*) Monocle2 heatmap showing gene expression of UPC and CD-related genes over pseudotime. (*E*) RNAscope on e18.5 mouse kidneys showing mutually exclusive expression of *Dmrt2* (yellow arrowheads) and *Hmx2* (white arrowheads) in Krt8^{+} cells of the UPC lineage. (*F*) B-IC associated coexpression of *Hmx2* and *Hmx3* in UPC-derived tubules within Six2TGC; tdTomato e18.5 kidneys. The orange arrowhead indicates tdTomato+ nephron lineage tubule. (*G*) Expression of *DMRT2* in *SLC4A1*-expressing A-ICs in week 18 fetal kidney (arrowhead). (*H*) Expression of *HMX2* in *SLC26A4*-expressing B- or nA/nB-ICs in week 18 fetal kidney (arrowhead). (*I*) Expression of *HMX2* in *SLC26A4* negative ICs in week 18 fetal kidney (arrowhead).

enrichment in the normal kidney (Dataset S2; https://cello.shin-yapps.io/kidneycellexplorer/). Thus, loss of *Hmx2/Hmx3* results in downregulation of gene activity associated with a B- and/or nA/nB-IC program and the corresponding upregulation of an early A-IC program. Collectively, the data are consistent with Dmrt2 directing an A-IC fate and Hmx2/Hmx3 directing a B- and/or

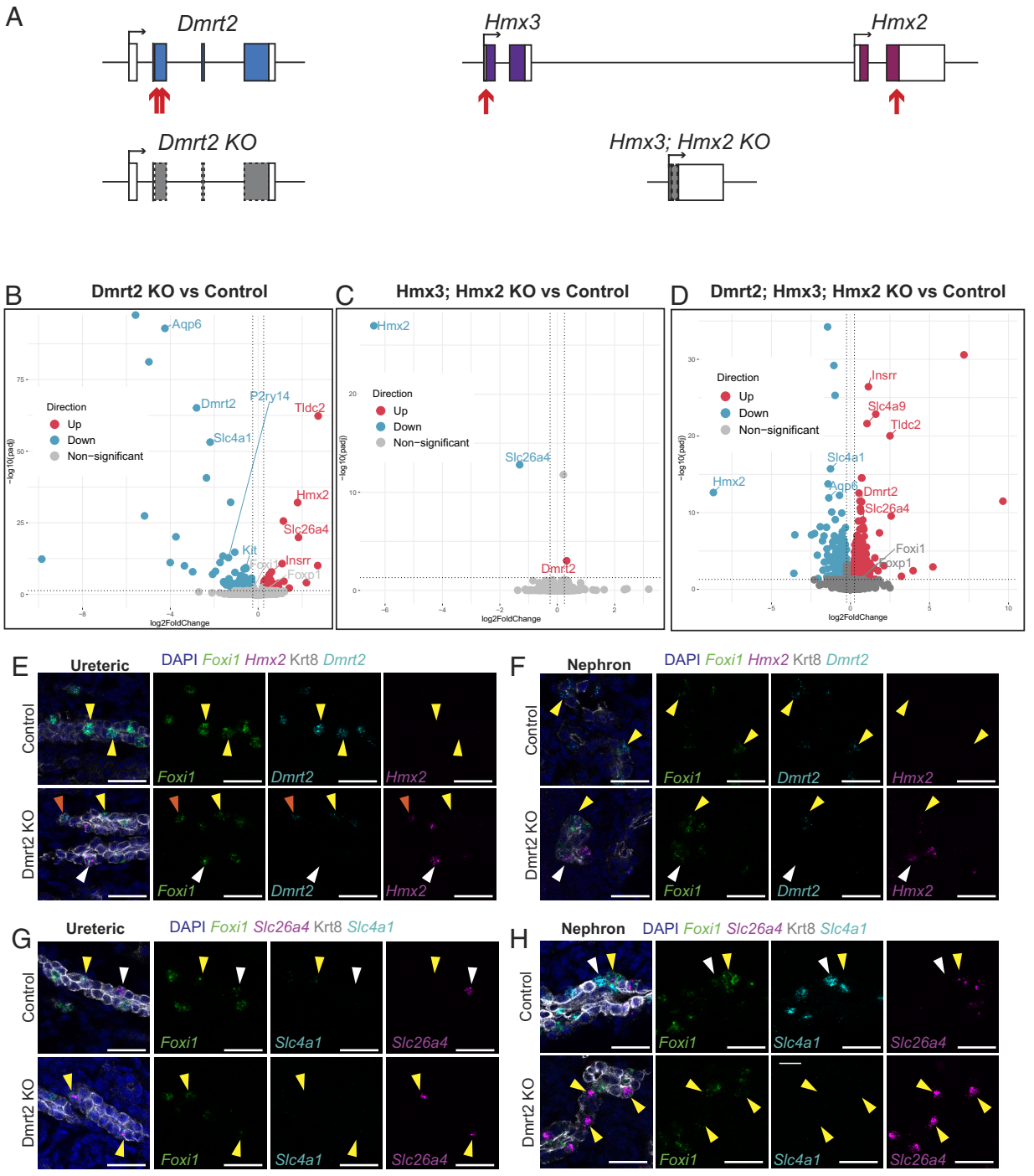

Fig. 2. Dmrt2 represses type B IC fates. (*A*) Schematic of CRISPR/Cas9 generated Dmrt2 and Hmx3/Hmx2 knockout alleles. Red arrows indicate sgRNA targeting sites. Gray boxes indicate out-of-frame coding sequence. (*B*) Differentially expressed genes comparing Dmrt2 knockout and wildtype kidneys at e18.5 (n = 3 each group). (*C*) Differentially expressed genes comparing Hmx2/Hmx3 knockout and wildtype kidneys at e18.5 (n = 6 each group). (*D*) Differential gene expression comparing Dmrt2/Hmx2/Hmx3 knockout and wild-type kidneys at e18.5 (n = 3). (*E*) Mutually exclusive expression of IC subtype-associated transcription factors Dmrt2 and Hmx2 in control and *Dmrt2* KO kidneys in the ureteric and (*F*) nephron lineages. Yellow arrowheads indicate *Dmrt2*$^+$ ICs; white arrowheads indicate *Hmx2*$^+$ ICs; orange arrowheads indicate rare Dmrt2$^+$/Hmx2$^+$ ICs. (*G*) Expression of IC bicarbonate transporters in the cortex of control and Dmrt2 KO kidneys. Yellow arrowheads indicate *Slc4a1*-expressing A-ICs; the white arrowhead indicates *Slc26a4*-expressing B-IC or nA/nB-ICs in ureteric or (*H*) nephron lineages (Scale bars, 25 μm) (OMZ = outer medullary zone, IMZ = inner medullary zone).

nA/nB-IC fate, with IC cells undergoing a cell fate switch on removal of a subtype-specific transcriptional regulator.

Analysis of *Dmrt2/Hmx2/Hmx3* triple mutant kidneys provided additional insight. Though triple mutants showed a broadly similar DEG profile to *Dmrt2* KO kidneys, expression of *Dmrt2* (a nonfunctional transcript) was significantly up-regulated in triple mutants contrasting with silencing of *Dmrt2* expression in *Hmx2*|*Hmx3* mutant kidneys (Fig. 2 *B* and *D* and Dataset S3). These data support a model in which Hmx2 and/or Hmx3 are required to silence *Dmrt2* expression. The deletion of *Hmx2/Hmx3* prevents an assessment of a potential role for Dmrt2 in silencing *Hmx2/3* expression.

To examine gene expression at the single-cell level in the kidney context, we selected genes from the DEG lists and analyzed their expression in situ with RNAscope. Although the actual relationship of radial domains in the late embryonic mouse kidney

relative to the adult mouse kidney are not clear, we used histological and gene expression criteria to distinguish "cortical," "outer medullary," (OMZ) and "inner medullary" zones (IMZ) (*SI Appendix*, Fig. S3*A*). In the cortical zone, A-, B-, and nA/nB-ICs are intermixed. Based on differences in tubule morphology, we distinguished the effect of Dmrt2 loss on *Dmrt2* and *Hmx2* expression in NPC or UPC-derived ICs. Cortically, we observed an increase in *Hmx2*-expressing ICs in both lineages on *Dmrt2* removal consistent with an A-IC to B- and nA/nB-IC transition (Fig. 2 *E* and *F*). A nonfunctional mutant *Dmrt2* transcript was detected in both cortical lineages but only in *Hmx2*$^-$ cells, with the exception of rare cells with weak expression of both Dmrt2 and Hmx2, potentially an early intermediate cell-type in the generation of IC heterogeneity (Fig. 2 *E* and *F*). In both cortical lineages, loss of *Dmrt2* was accompanied by a loss of *Slc4a1*-expressing ICs and an increase in those expressing *Slc26a4* (Fig. 2 *G* and *H*), as observed on *Dmrt2* removal from the mature kidney (26). Together these data are consistent with Dmrt2 promoting A-IC fates and suppressing an alternative Hmx2-directed program.

The medullary zone comprises almost exclusively A-IC types (32). Consistent with a switch in IC subtype fate paralleling cortical UPC derivatives, *Hmx2* and *Slc26a4* were ectopically activated in *Foxi1*$^+$/*Dmrt2*$^-$/*Slc4a1*$^-$ ICs in the OMZ (Fig. 3 *A* and *B*). In contrast, in the IMZ, Foxi1$^+$ ICs maintained *Dmrt2* expression, lost *Slc4a1* expression, and failed to activate ectopic expression of *Hmx2* or *Slc26a4* (Fig. 3 *C* and *D*). These data point to an additional layer of regional regulation of IC programs in the IMZ: a positive role for Dmrt2 in maintaining *Slc4a1* expression and the absence of an *Hmx2* promoting factor or presence of an *Hmx2* inhibitory factor. Analyzing *Hmx2/Hmx3* mutant kidneys revealed a slight increase in *Dmrt2*$^+$/*Foxi1*$^+$ ICs in the nephron lineage (Fig. 3 *E* and *F*); cortical UPC-derived B-ICs were only rarely observed in wild-type kidneys at this stage (Fig. 3*G*). No *Slc26a4*$^+$/*Foxi1*$^+$ ICs were evident (Fig. 3*H*) consistent with the downregulation of *Slc26a4* observed in mRNA-seq analysis (Fig. 2*C*).

Strikingly, RNAscope analysis of cortical ICs in e18.5 *Dmrt2/Hmx2/Hmx3* triple mutant kidneys identified ICs coexpressing *Slc4a1* and *Slc26a4* (Fig. 4*A* and *SI Appendix*, Fig. S4 *A–F*). To unambiguously distinguish the origin of these hybrid ICs, we examined Hox gene profiles which distinguish between the different temporal and spatial origins of NPCs and UPCs[2]. *Hoxd10* expression specifically identifies ICs derived from the nephron lineage that are consequently restricted to the cortex (*SI Appendix*, Fig. S4 *G* and *H*). *Hoxd10* expression in *Slc4a1*$^+$/*Slc26a4*$^+$ hybrid ICs indicated these originated from the NPC lineage in triple mutants, pointing to lineage-associated differences in IC regulatory programs (Fig. 4 *B* and *C*). In contrast to *Dmrt2* mutant kidneys where ectopic activation of *Hmx2* in the OMZ correlated with a loss of *Dmrt2* expression, *Dmrt2* was activated in the OMZ and IMZ of triple mutants (Fig. 4 *D–G* and *SI Appendix*, Fig. S4 *A* and *B*). As with the *Dmrt2* mutant, triple mutant OMZ ICs were Slc4a1$^-$/Slc26a4$^+$, and IMZ ICs were Slc4a1$^-$/Slc26a4$^-$ (Fig. 4 *G–K* and *SI Appendix*, Fig. S4 *C* and *D*). Thus, *Hmx2/Hmx3* were not essential for ectopic *Slc26a4* expression in OMZ ICs of the triple mutant.

Ectopic Expression of *Dmrt2* and *Hmx2* in UPC-Derived Organoid Cultures. To extend the analysis of *Hmx2/Hmx3* mutants to obtain additional insight into their roles in UPC derivatives and to further analyze *Dmrt2* and *Hmx2* regulatory activity, we turned to a mouse collecting duct organoid culture system (37). e11.5 ureteric buds (UB) were isolated from wild-type controls and *Hmx2/Hmx3* mutants, expanded for 10 d in progenitor maintenance conditions, then allowed to differentiate for 7 d (*Materials and Methods*) (37). Relative to the wild-type controls, mutants showed an expected, loss of *Hmx2* and *Hmx3* expression, and though not significant, *Slc26a4* expression trended downward, and *Dmrt2* and *Slc4a1* expression upward, in mutant kidney organoids (*SI Appendix*, Fig. S4*I*). Generally, these data are consistent with observations of the NPC lineage in *Hmx2/Hmx3* mutant kidneys, that *Hmx2/Hmx3* promoted an B-IC fate and suppressed the initiation of an A-IC program.

To examine the activity of transcriptional regulators in IC programs more directly, we infected ureteric epithelial organoids with doxycycline(dox)-inducible lentivirus driving the expression of i) mCherry (control), ii) *Foxi1*, iii) *Foxi1* and *Dmrt2-Flag*, or iv) *Foxi1* and *Hmx2-Flag* (Fig. 5*A* and *SI Appendix*, Fig. S5*A*). Immunostaining confirmed robust, dox-dependent detection of Foxi1 and each of the epitope-tagged transcription factors (*SI Appendix*, Fig. S5*B*). Infected UB organoids were cultured in a modified medium with aldosterone and vasopressin which promotes PC but not IC development (38) (Fig. 5*B* and *SI Appendix*, Table S1). In agreement with published studies (37), we observed an upregulation of *Aqp2* indicative of PC programming (*SI Appendix*, Fig. S5*C*), while background IC development was minimal; less than 3% of cells showed detectable *Foxi1* (*SI Appendix*, Fig. S5 *D* and *E*). Coexpression of *Dmrt2* in these cells suggested a predisposition to A-IC development, reflecting the temporal program of IC specification in the UPC lineage in vivo (*SI Appendix*, Fig. S5 *E* and *F*).

Induction of *Foxi1* led to a pronounced upregulation of *Dmrt2* in a subset of *Foxi1*$^+$ cells (Fig. 5 *C*, *D*, and *J*), a modest but significant upregulation of *Hmx2* (Fig. 5*J*), and a nonsignificant increase in *Slc4a1* and *Slc26a4* by qRT-PCR, though neither could be detected by RNAscope (Fig. 5 *C–J*). In contrast, Atp6v1b1, a IC restricted component of the vacuolar ATPase regulating acidification in all IC-types, was observed by immunodetection in 85% of Foxi1$^+$ cells 3 d post dox addition, an optimum time for assaying the acute response to Foxi1 induction (*SI Appendix*, Fig. S5 *G–I*). On coinfection with *Foxi1* and *Dmrt2,* a weak upregulation of *Slc4a1* was detected by qPCR (*SI Appendix*, Fig. S5*J*); however, dox induction resulted in an *Slc4a1* transcript readily visualized by RNAscope in situ hybridization and downregulation of *Hmx2* and *Slc26a4* (Fig. 5 *F*, *H*, and *J* and *SI Appendix*, Fig. S5*J*). Dox induction of *Foxi1* and *Hmx2* led to the downregulation of *Dmrt2* and *Slc4a1* expression (Fig. 5 *C*, *D*, *F*, *H*, and *J* and *SI Appendix*, Fig. S5*J*) and RNAscope revealed an upregulation of *Slc26a4* in a subset of *Foxi1*$^+$ *Hmx2*$^+$ cells (Fig. 5 *G*, *I*, and *J* and *SI Appendix*, Fig. S5*J*). Collectively, these data support in vivo observations of Dmrt2 promoting an A-IC fate and suppressing an B-IC fate and Hmx2 playing an opposite role promoting an IC-B fate while suppressing an A-IC fate.

Discussion

The NPC-derived connecting segment and UPC-derived collecting epithelium play central roles in regulating the homeostasis of the body's fluids through the actions of PC and IC types (1, 2, 29). A transcriptional hierarchy governing the specification of principal and IC cells has emerged from genetic studies. For the IC cell lineage, Tcfp2l1, Foxp1, and Foxi1 are essential for the specification of ICs, though only Foxi1 is restricted to the IC lineage (13, 26, 39, 40). Ectopic expression of FOXI1 in a human UPC organoid model is sufficient to induce B-IC development (38). In contrast, we observed induction of Foxi1 in the mouse UPC organoid model results in a marked upregulation of A-IC features. Given similar culture conditions in these two studies, the

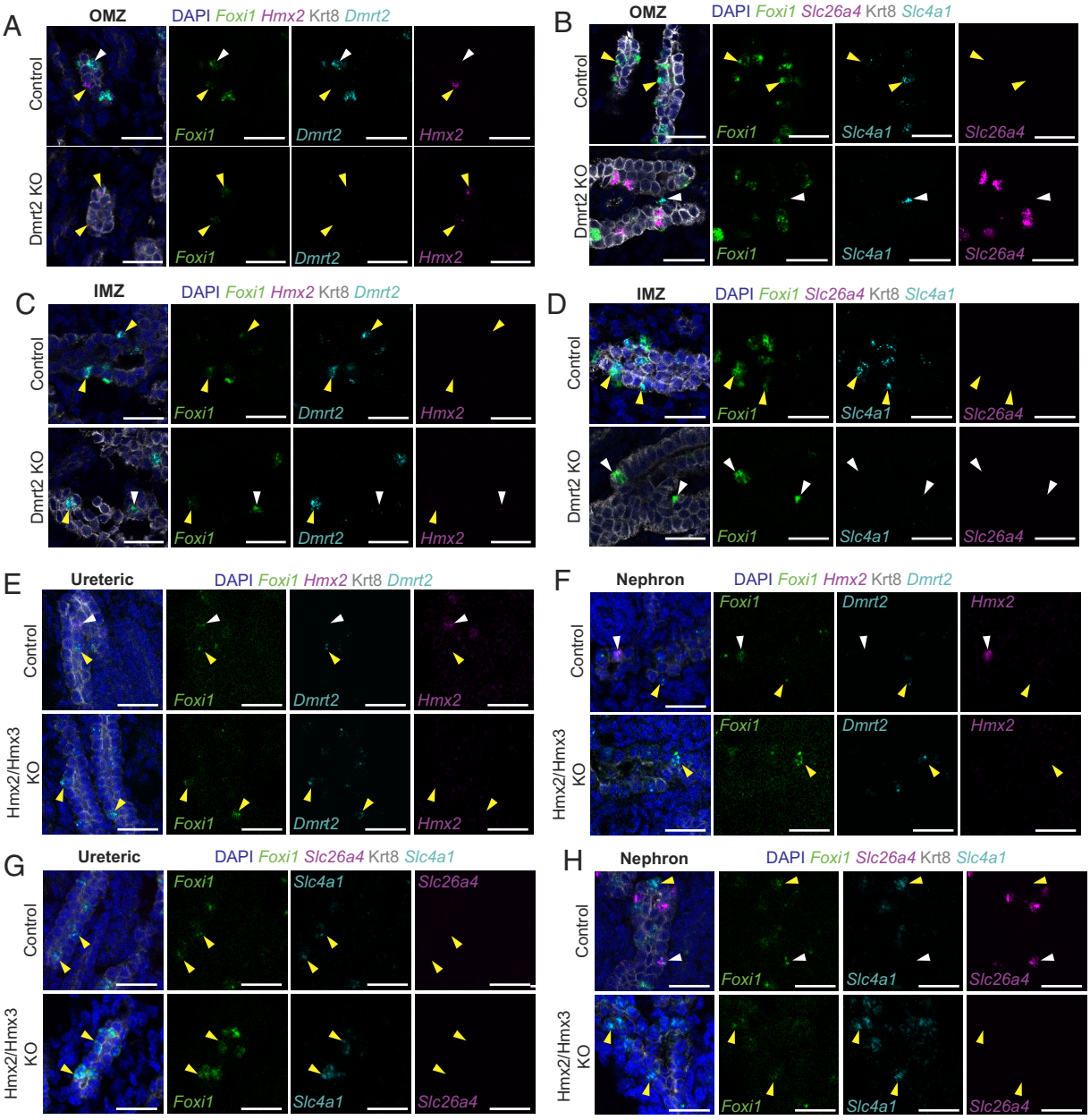

Fig. 3. Loss of Dmrt2 reveals region-specific regulation of IC fate. (*A*) Expression of IC subtype-associated transcription factors in control and *Dmrt2* KO kidneys in the OMZ. Yellow arrowheads indicate *Hmx2*-expressing ICs; white arrowheads indicate *Dmrt2*-expressing ICs. (*B*) Expression of A-IC (yellow arrowheads) and B-IC markers in the OMZ of control and *Dmrt2* KO kidneys. The white arrowhead denotes non-nucleated red blood cells. (*C*) Expression of IC subtype-associated transcription factors in the IMZ of control and *Dmrt2* KO kidneys. Yellow arrowheads indicate *Dmrt2*-expressing ICs; the white arrowhead indicates *Foxi1*$^{+}$/*Dmrt2*$^{-}$/*Hmx2*$^{-}$ IC. (*D*) Expression of type A (yellow arrowheads) and type B IC markers in the IMZ of control and Dmrt2 KO kidneys. White arrowheads indicate *Foxi1*$^{+}$/*Slc4a1*$^{-}$/*Slc26a4*$^{-}$ IC. (*E*) *Dmrt2* and *Hmx2* expression in ureteric and (*F*) nephron cortical collecting duct and connecting tubule, respectively in e18.5 *Hmx2/Hmx3* KO kidneys. Yellow arrowheads denote *Foxi1*$^{+}$/*Dmrt2*$^{+}$ ICs; white arrowheads denote *Foxi1*$^{+}$/*Hmx2*$^{+}$ ICs. (*G*) Expression of intercalated cell bicarbonate transporters in the cortex of control and *Hmx2/Hmx3* KO kidneys. Yellow arrowheads indicate *Foxi1*$^{+}$/*Slc4a1*$^{+}$ A-ICs; white arrowheads indicate *Foxi1*$^{+}$/*Slc26a4*$^{+}$ B-ICs or nA/nB-ICs in ureteric or (*H*) nephron lineages (Scale bars, 25 μm) (OMZ = outer medullary zone, IMZ = inner medullary zone).

different outcomes suggest species differences in epithelial responsiveness to Foxi1. In the mouse, specification of A-ICs predominates in the early ureteric collecting epithelium, consistent with a medullary to cortical maturation process that allows for a functional though developmentally immature kidney at birth (32). In humans, there is an in utero period of 8 to 12 wk following the cessation of nephrogenesis which may permit a distinct IC program. Postspecification, a Notch signaling axis from ICs to PCs, inhibiting a PC to IC transition, maintains a balance between these cell types (27–30). We have extended the analysis of regulatory programs directing IC cell fate identifying Dmrt2 and Hmx2/Hmx3 as critical determinants of IC subtype specificity.

IC subtypes differ in origin (NPC or UPC lineage) and position occupied in the kidney (cortical and/or medullary zone). Our study argues for a general role of Dmrt2 in specification of A-ICs (NPC and UPC-derived) and Hmx2/Hmx3 in the specification of B- and nonA/nonB-IC (UPC and NPC-derived respectively) types. Mutual exclusivity in the expression of Dmrt2 and Hmx2/Hmx3 at the onset of IC development in the mouse and human kidney suggests a model in which these factors inhibit alternative pathways of IC development through corepression. This conclusion is supported by genetic data in our study. Further, analysis of Dmrt2 activity in the mature kidney suggests an ongoing role post-IC specification in A-ICs repressing Hmx2 and B-IC

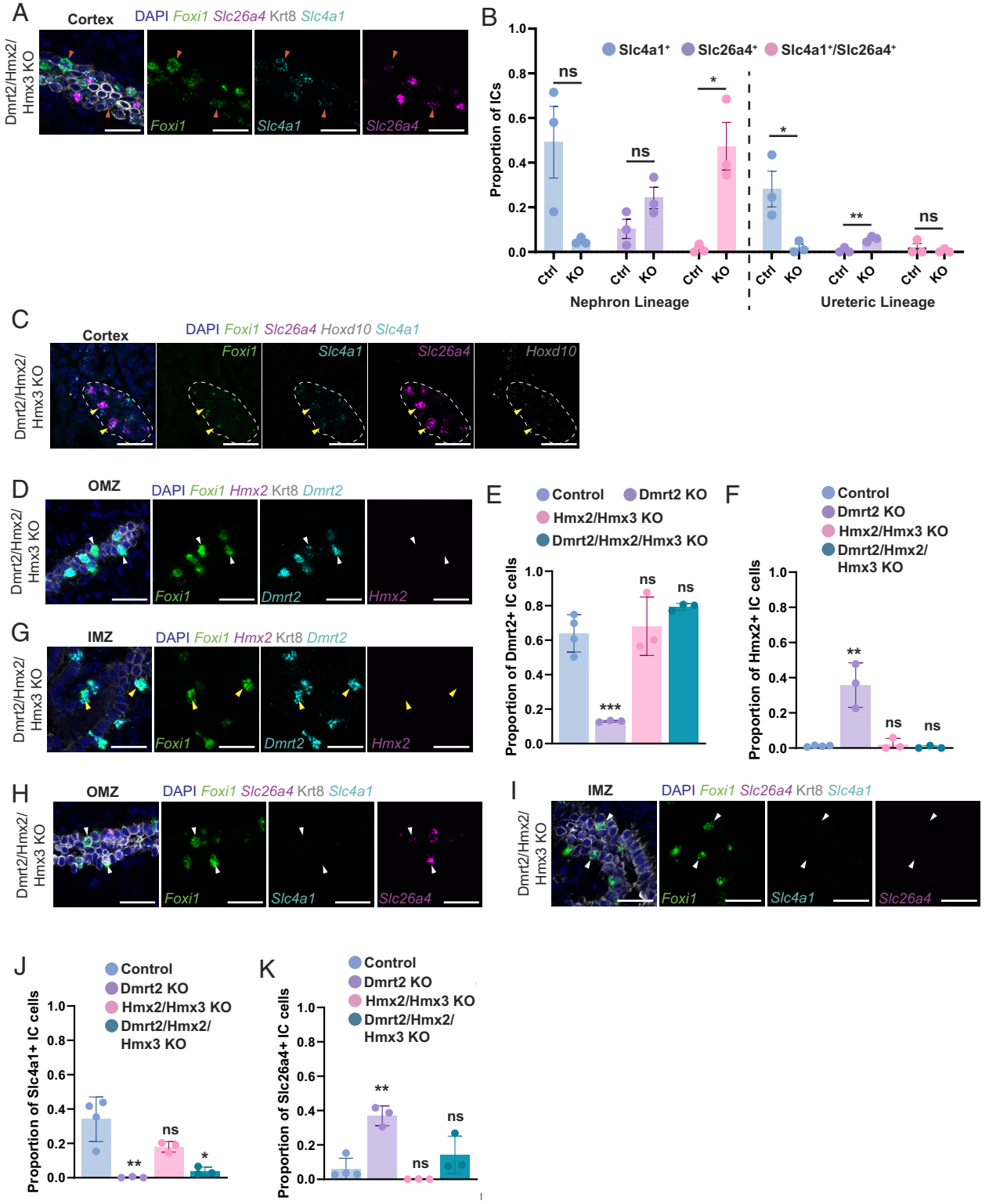

Fig. 4. *Dmrt2/Hmx2/Hmx3* knockout kidneys contain hybrid IC fates. (*A*) Expression of A- and B-/nA/nB-IC markers in the cortex of triple knockout kidneys at e18.5. Orange arrowheads indicate *Foxi1*$^+$/*Slc4a1*$^+$/*Slc26a4*$^+$ hybrid ICs. (*B*) Quantification of *Slc4a1*$^+$, *Slc26a4*$^+$, and *Slc4a1*$^+$/*Slc26a4*$^+$ ICs derived from nephron or ureteric lineages in the cortex of control and triple knockout kidneys. (*C*) Expression of nephron lineage marker *Hoxd10* in *Foxi1*$^+$/*Slc4a1*$^+$/*Slc26a4*$^+$ ICs within triple knockout kidneys (yellow arrowheads). The white dashed line outlines tubule boundaries. (*D*) Expression of *Dmrt2* and *Hmx2* in the OMZ of triple knockout kidneys at e18.5. White arrowheads indicate *Hmx2*$^+$ ICs. (*E*) Quantification of the proportion of *Dmrt2*$^+$/*Foxi1*$^+$ and (*F*) *Hmx2*$^+$/*Foxi1*$^+$ cells out of total *Foxi1*$^+$ cells in control, *Dmrt2* knockout, and *Dmrt2/Hmx2/Hmx3* knockout kidneys (n = 3 for each condition). (*G*) Expression of Dmrt2 and Hmx2 in the IMZ of triple knockout kidneys at e18.5 Yellow arrowheads denote *Foxi1*$^+$/*Dmrt2*$^+$/*Hmx2*$^-$ cells. (*H*) Expression of A- and B-IC markers in the OMZ of triple knockout kidneys at e18.5. White arrowheads indicate *Foxi1*$^+$/*Slc4a1*$^-$/*Slc26a4*$^+$ B-ICs. (*I*) Expression of A- and B-/nA/nB-IC markers in the IMZ; white arrows indicate *Foxi1*$^+$/*Slc4a1*$^-$ ICs. (*J*) Quantification of *Slc4a1*$^+$/*Foxi1*$^+$, or (*K*) *Slc26a4*$^+$/*Foxi1*$^+$ cells out of total *Foxi1*$^+$ cells in control, *Dmrt2* knockout, and *Dmrt2/Hmx2/Hmx3* knockout kidneys (n = 3 for each condition) (significance was determined using the Student's *t* test compared to control condition; *$P \le 0.05$, **$P \le 0.01$, ns = nonsignificant) (Ctrl = Control, KO = *Dmrt2/Hmx2/Hmx3* KO).

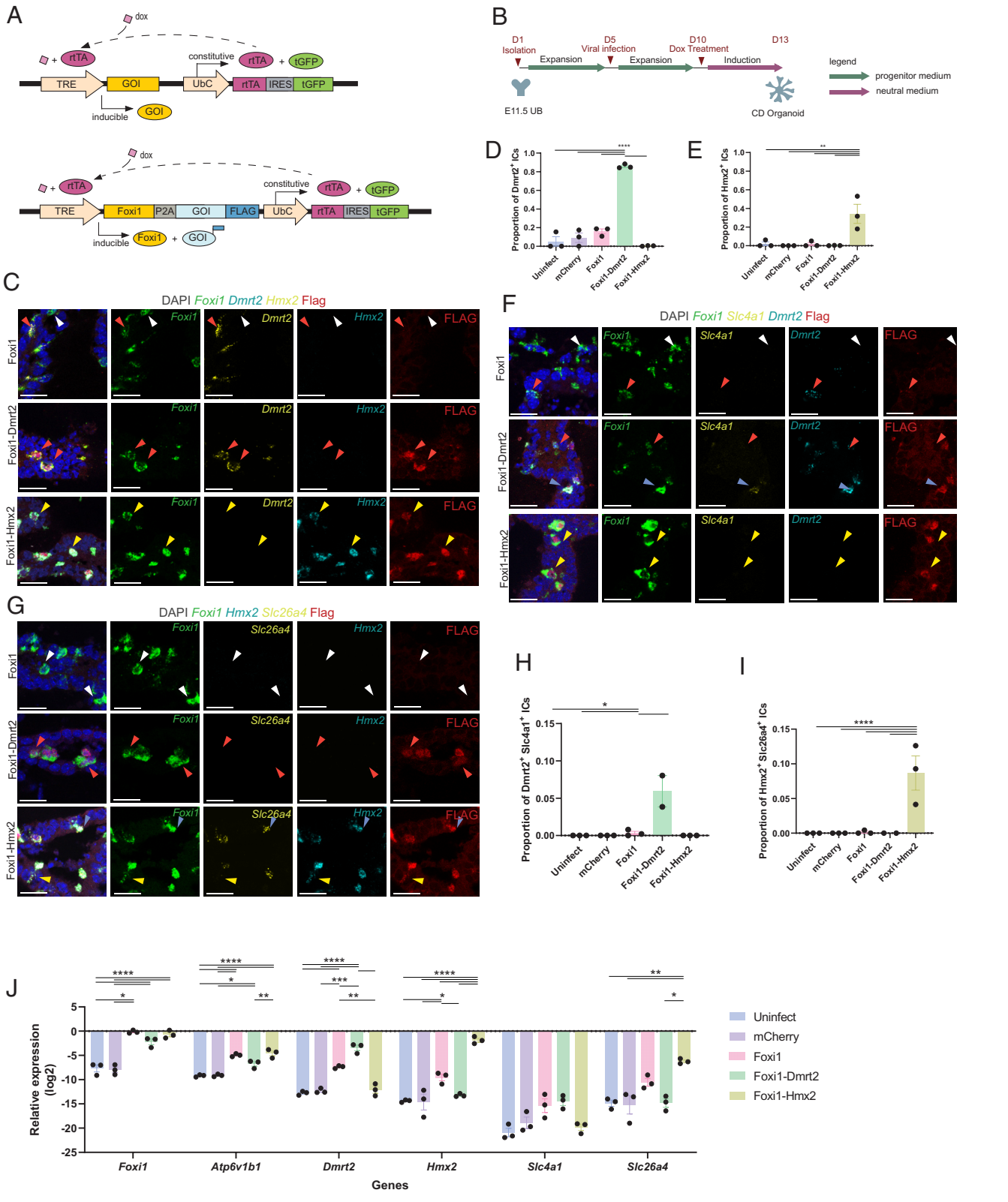

Fig. 5. Overexpression of Dmrt2 and Hmx2 in UPC-derived collecting epithelial organoid culture promotes type A and B cell fate, respectively. (*A*) Map of the virus constructs. *Top* indicates monocistronic virus—GOI (gene of interest) either "*mCherry*" or "*Foxi1*"; *Bottom* indicates bicistronic viruses—GOI either "*Dmrt2*" or "*Hmx2*." (*B*) Schematic of organoid culture workflow. (*C*) RNAscope images of *Foxi1, Dmrt2, Hmx2*, and FLAG in dox-treated organoid cultures; white arrowheads indicate *Foxi1*$^+$ cells; orange arrowheads indicate *Foxi1*$^+$/*Dmrt2*$^+$ cells; yellow arrowheads indicate *Foxi1*$^+$/*Hmx2*$^+$ cells. (*D*) Quantification of *Dmrt2*$^+$/*Foxi1*$^+$ *ICs* and (*E*) of *Hmx2*$^+$/*Foxi1*$^+$ ICs out of total *Foxi1*$^+$ICs in dox-treated organoid cultures. (*F*) RNAscope images of *Foxi1, Dmrt2, Slc4a1*, and FLAG; white arrowheads indicate *Foxi1*$^+$ cells; orange arrowheads indicate *Foxi1*$^+$/*Dmrt2*$^+$ cells; blue arrowheads indicate *Foxi1*$^+$/*Dmrt2*$^+$/*Slc4a1*$^+$ cells; yellow arrowheads indicate *Foxi1*$^+$/*Hmx2*$^+$ cells. (*G*) RNAscope images of *Foxi1, Hmx2, Slc26a4*, and FLAG in dox-treated organoid cultures; white arrowheads indicate *Foxi1*$^+$ cells; orange arrowheads indicate *Foxi1*$^+$/*Dmrt2*$^+$ cells; yellow arrowheads indicate *Foxi1*$^+$/*Hmx2*$^+$ cells; blue arrowheads indicate *Foxi1*$^+$/*Hmx2*$^+$/*Slc26a4*$^+$ cells. (*H*) Quantification of *Dmrt2*$^+$/*Slc4a1*$^+$/*Foxi1*$^+$ *ICs* and (*I*) of *Hmx2*$^+$/*Slc26a4*$^+$/*Foxi1*$^+$ ICs out of total *Foxi1*$^+$ICs in dox-treated organoid cultures. (*J*) Relative expression of generic and subtype IC genes normalized to *Gapdh* in dox-treated organoid cultures. (Significance was determined by one-way ANOVA; *$P \le 0.05$, **$P \le 0.01$, ***$P < 0.001$, ****$P < 0.0001$. Significance not indicated on the graph is nonsignificant; Scale bar, 25 μm for all RNAscope images.)

development (26). Mechanisms of corepression direct local specification of neural progenitor subtypes in response to Hedgehog signaling in patterning the vertebrate neural tube (41). Our studies suggest a more complex role for IC regulatory factors than simply silencing alternative programs. Genetic removal in vivo and ectopic expression studies in vitro point to positive roles for Dmrt2 in promoting expression of A-IC gene activity and Hmx2 in promoting B-IC gene activity.

How these factors may operate as both repressors and activators is unclear. In vivo analysis points to lineage and regional variability in regulatory outcomes. The coactivation of *Slc4a1* and *Slc26a4* in triple mutant ICs devoid of *Dmrt2*, *Hmx2,* and *Hmx3* activity is restricted to cortical NPC-derived NPCs. Thus, in this lineage, there is no absolute requirement for *Dmrt2* or *Hmx2* for the expression of critical bicarbonate transporters normally restricted to distinct IC subtypes. This contrasts with the UPC lineage in which *Dmrt2* is required for induction of *Slc4a1*. Further, whereas in the OMZ loss of *Dmrt2* in A-IC cells results in the ectopic activation of *Hmx2* and *Slc26a4*, and silencing of *Dmrt2* and *Slc4a1*, indicative of an A- to B-type IC conversion, IMZ ICs maintain a Dmrt2$^+$ A-IC identity, though without a functional Dmrt2 transcript, IMZ cells fail to activate a *Dmrt2*-dependent A-IC program.

Collectively, these studies suggest distinct regulatory programs within cell lineages and local environmental interplay in cortical and medullary regions, modifying regional IC patterning processes in the developing kidney. Medullary B-ICs detected during development undergo apoptosis during postnatal development to become restricted to the cortex (32, 33), although the signals that drive this are unknown. Additionally, the transcription factor Nfat5, which is regulated through phosphorylation and expressed beyond the medullary region, has increased activity in the kidney medulla in response to hypertonicity (42). Nfat5 knockout mice have significantly reduced expression of *Slc4a1* and other type A IC markers, supporting a role for Nfat5 in the control of medullary IC programs (43).

Analysis of an ongoing requirement for *Dmrt2* in the mature kidney suggests a continued requirement for maintaining A-ICs (26). A potential for switching of IC-types in association with acid load indicates additional mechanisms upstream of IC subtype determinants to regulate the regional composition of IC subtypes in the adult kidney (44). Previous work documented a specific role for the extracellular protein Hensin/Dmbt1 in the generation of A-ICs (15, 45). *Dmbt1* knockout mice show increased Slc26a4 in the kidney cortex suggestive of B-IC conversion. In the medulla, ICs lose A-IC features, show ultrastructural characteristics of B-ICs, but do not produce Slc26a4 (15). No significant change in expression of *Dmbt1* was observed in RNA-seq of *Dmrt2* knockouts, suggesting that *Dmbt1* is regulated independently of Dmrt2.

In summary, our studies point to the interplay of Dmrt2, Hmx2, and Hmx3 in specification of IC subtypes in the developing mammalian kidney, downstream of *Tfcp2l1*, Foxi1, and *Foxp1* which play a more general role in IC specification (13, 26, 27). In the adult kidney, PC to IC interconversion and diet-induced modification of IC subtypes suggest continued flexibility within gene regulatory programs maintaining ICs (1, 27–30). The Notch pathway plays a critical role in PC to IC interconversion though the transcriptional control mechanisms at play have not been determined and may not necessitate a direct interplay with subtype diversity pathways. In contrast, diet-dependent mechanisms controlling plasticity in IC cell subtypes could be expected to interact directly with IC subtype specifying programs. Future studies to enhance an understanding of developmental processes and regulatory plasticity in the adult kidney will benefit from the identification of transcriptional complexes and DNA target associations underlying the actions of Dmrt2, Hmx2, and Hmx3.

Materials and Methods

Animal Care and Use. The animal work in this study was reviewed and approved by the Institutional Animal Care and Use Committees (IACUC) at the University of Southern California. Experiments as performed adhered to institutional guidelines. CRISPR/Cas9-generated lines were generated as described below. Animals were bred together in heterozygous intercrosses, and females were checked for plugs to generate staged embryos. Kidneys were extracted from staged embryos for subsequent analysis.

CRISPR sgRNA Design. sgRNA for editing targets were designed using the Synthego ICE CRISPR design tool and ordered from Synthego. See *SI Appendix, Supplemental Materials* for sgRNA sequences.

Electroporation. Gene editing on zygotes was performed as previously described (46). Briefly, fertilized eggs were recovered from superovulated, the zona pellucida was removed and embryos were electroporated with preformed CAS9/gRNA complexes (47).

Sanger Sequencing and Cloning Analysis to Validate CRISPR-Generated Lines. GXL Taq Polymerase was used to amplify target sequence PCR products from founder mice. PCR conditions were optimized to give one PCR product from primer sets (see *SI Appendix, Supplemental Materials* for primer sequences). PCR products were run on gel electrophoresis and products were gel extracted using the QIAQuick Gel Extraction Kit and sent for Sanger sequencing via Genewiz. Results were aligned in A Plasmid Editor (48) to look for sequence mismatches and insertions. Trace files were also examined for evidence of small deletions. In the cases where alignments were inconclusive, TOPO cloning was performed; 12 clones were picked per sample, expanded in liquid culture, Sanger sequenced, and aligned to identify desirable alleles.

After PCR, cloning, and alignment analysis was performed, founding mice were selected and crossed to C57BL6/J mice to identify progeny from the F1 with the desired allele. F1 generated mice were both genotyped and sequenced until F2 progeny were established with the desired allele for transmission, then exclusively genotyping primers were used to genotype progeny. Genotyping primer sequences, sequence information, and sgRNA sequences can be found in Supplemental Materials.

Single-Cell RNA Sequencing Analysis. Analysis of published single-cell sequencing data from P0 mouse kidneys (GSE232482), human fetal, or pediatric samples was performed using Seurat v4 packages. For the human fetal data, clusters encoding cells of the ureteric lineage were identified through manual annotation and subclustered to identify intercalated cell types. Subclustering analysis was performed by using the "subset" function for *Foxi1*$^+$ or *FOXI1*$^+$ clusters. The GEO accession number for the human fetal ureteric lineage object is GSE295893 (49).

Monocle2 Pseudotime Analysis. Pseudotime analysis was performed using Monocle2 (50–52) packages. From P0 single-cell RNA sequencing (31), we subclustered collecting duct cell types including progenitor and differentiating cells as previously described (32), subsetting ureteric lineage cells only through Hox gene expression (2, 12). Foxi1+ IC clusters and progenitors, as well as Tfcp2l1+/Aqp2− differentiating cells were isolated and processed through Monocle2. A heatmap was generated to visualize gene expression over pseudotime for key genes related to IC subtype differentiation.

Identification of Mouse Transcription Factors. The curated list of human transcription factors was converted into mouse orthologs using OrthoRetriever (https://lighthouse.ucsf.edu/orthoretriever). This list of "mouse" transcription factors was cross referenced to the differentially expressed gene list generated from P0 IC clusters from the entire ureteric lineage object (31) and the resulting transcription factors were visualized on a dotplot.

Tissue Preparation. Samples were prepared as previously described (32). Briefly, one kidney per biological replicate was fixed in 4% paraformaldehyde on ice for 20 to 30 min and incubated in 30% sucrose overnight. After embedding in Optimal Cutting Temperature, samples were sectioned at 12 μm for histological analyses.

Immunofluorescence. Slides were stained as previously described (32), using either 0.1% Triton-X100/PBS or 0.1% Tween-20/TBS.

RNAscope Detection of Transcripts. The RNAscope Multiplex Fluorescent v2 Assay was performed according to the manufacturer's published protocol for fixed frozen tissue with some modifications as previously described (32).

Immunofluorescent Slide Imaging. Immunofluorescent and RNAscope slides were imaged at 40× on Leica Sp8 DLSM confocal microscope. For RNAscope and immunofluorescent slides, tile scan images were captured at 40× for n = 3 biological replicates for each condition with laser conditions optimized for each sample to reasonably capture the full intensity spectra; for all kidney sections, imaging coverage was over 50% of the section, including all corticomedullary zones. For all collecting duct organoid sections, the entire organoid was imaged.

RNAscope Image Quantification. QuPath was used to quantify cells with positive signal (puncta) for Foxi1, Dmrt2, Hmx2, Slc4a1, or Slc26a4 after RNAscope detection of transcripts. Full tilescan images were used for analysis; an average of 370 Foxi1$^+$ ICs were quantified per kidney section and an average of 273 Foxi1$^+$ ICs were quantified per organoid section. Individual channel images were exported from RNAscope LASX .lif files and made into stacks in ImageJ. Files were converted to 8-bit and remerged. Tiff stacks were imported into QuPath and pixel height/width were both assigned as 0.284 μm, in accordance with pixel size from original images. Annotation regions were drawn to cover cortical, outer, and inner medullary boundaries. The distinction between inner and outer medulla was approximated roughly based on tubule diameter (larger diameters indicating inner medullary compartments). Cell detection was used with default parameters on the DAPI channel, except for maximum object size = 50, and minimum threshold = 2 to 5, depending on the image. Subcellular detection was used with thresholds based on the controls. Cell detections were exported as .csv files. Cells that had >0 number of subcellular detections were counted as positive for each channel. Foxi1$^+$ and any subtype-specific marker (Dmrt2, Hmx2, Slc4a1, or Slc26a4) positive cells were summed and divided by the total number of Foxi1 positive cells for each sample/region. The proportion of Foxi1$^+$/subtype marker$^+$ cells was plotted in GraphPad Prism 9.5.0 (n = 3 for each condition).

Bulk RNA Sequencing Analysis. Kidneys were extracted from e18.5 pups; tail samples were collected for genotyping. One kidney was preserved in RNAlater and stored at −80 °C until RNA extraction was performed using the Qiagen RNeasy Mini Kit according to the manufacturer's instructions with all optional steps. RNA was eluted in 30 μL of nuclease-free water and stored at −80 °C until sent to the Genome Access Technology Center at the McDonnell Genome Institute in Washington University at St. Louis for library preparation and sequencing. Library preparation was performed using a PolyA selection step. Samples were sequenced on the NovaSeq S4 for 150 bp paired end reads. Raw files were aligned and filtered as previously described (53). Differential expression analysis was performed using DESeq2 in R. Standard cutoffs of log2FC (0.25) and adjusted *P*-value (0.05) were used to identify statistically significant gene expression changes. Raw fastq files and read counts can be found at GEO: GSE274904.

Lentivirus Generation. Constructs for lentiviral transduction were generated using Gibson Assembly; primers for assembly and adding epitope tags were designed using Snapgene. PCR products were gel extracted and validated through Sanger Sequencing and cloned into pInducer22 via In-fusion cloning. Products were transformed into Stellar Chemically Competent Cells. Cells were spread on Ampicillin-coated agar plates in S.O.C. medium and incubated overnight at 37 °C. Clones were picked and grown in shaking liquid culture (230 rpm) in Luria Broth (LB) with Ampicillin (100 μg/mL) overnight at 37 °C. Midi prep was performed according to the manufacturer's instructions and the resulting transfer, envelope, and packaging vectors were transfected into HEK293T cells in growth medium (10% FBS/DMEM). The supernatant was harvested twice after 48 and 72 h posttransfection; Lenti-x concentrator was used to concentrate virus for future transduction. Viruses were titrated using a lentivirus quantification kit.

Lentivirus Infection into Fibroblasts. Human fibroblasts were derived from H9 ESCs purchased from WiCell (WA09) using a previously reported protocol (54). Human fibroblasts were infected with lentiviruses using polybrene (5 μg/mL) (Sigma, cat. TR-1003) in 10% FBS/DMEM. Viruses were removed 24 h postinfection, and 1% pen strep was added to the medium with 1 μg of dox. Cells were assayed with immunofluorescence 72 h postinfection.

Organoid Culture. Mouse UBs were isolated from E11.5 kidneys, cultured for 5 d in vitro in the progenitor medium, and infected with viruses as described previously (37). Briefly, organoids were dissociated on D5 post-UB isolation using Accumax and infected with lentiviruses with polybrene (5 μg/mL) by spinoculation at 800×*g* for 15 min. Infected cells were aggregated overnight with 10 μM Y27632, which was removed 24 h postaggregation. Organoids were re-embedded in Matrigel and continuously cultured in the progenitor medium for expansion. On D5 postinfection, organoids were switched to the neutral medium consisting of DMEM/F12, 1% pen strep, 1X GlutaMAX, 1X MEM-NEAA, 0.1 mM 2-mercaptoethanol, 1X B-27 minus vitamin A, 1X ITS, 10 nM aldosterone, and 10 nM vasopressin. In this neutral medium, organoids were also treated with 1 μg of doxycycline every other day. They were harvested on D3 post-dox administration.

Organoid Preparation for Histological Analyses. Organoids were processed as previously described (37). Briefly, organoids were fixed with 4% PFA for 5 min on ice and rinsed 3× in PBS for 5 min each wash. Samples were incubated in 30% sucrose overnight and embedded in optimal cutting temperature. Once embedded, organoids were sectioned at 7 μm for histological analyses.

Tissue storage and single-nuclei isolation. Following protocol review by USC's Institutional Review Board, deidentified, consented fetal kidneys (Obstetrics and Gynecology Maternal Fetal Medicine Division of University of Southern California) were finely minced on ice, then placed in ice cold Nuclei EZ Lysis Buffer (Sigma, N3408) supplemented with protease inhibitor (Roche, 05892791001) and cells broken by dounce homogenization with 15 loose strokes in a loose pestle and tight pestle system (Sigma, P0485). Following filtration through a 200 μm strainer (pluriSelect, 43–50200), the homogenate was subjected to an additional 5 strokes with the tight pestle, incubated on ice for 5 min, filtered through a 40 μm strainer (pluriSelect, 43–50040), then centrifuged at 500 x g for 5 minutes at 4 °C in a swinging-bucket centrifuge. The nuclear pellet was resuspended in Nuclei EZ Lysis Buffer, incubated on ice for an additional 5 min, centrifuged, and the final pellet was resuspended in chilled 1X Nuclei Buffer (10x Genomics, 2000297) and filtered through a pre-wetted 5 μm filter (pluriSelect 43-50005). All nuclear isolation reagents contained Protector RNAse inhibitor (Promega, N2615) at a final concentration of 1 U/μl and DTT (Sigma 6465663) at a final concentration of 1 mM.

Multiome Sequencing and analysis. Single-nucleus RNA-sequencing and ATAC-sequencing libraries were generated using the 10X Genomics Chromium Next GEM Single Cell Multiome reagents (PN-1000283) following the manufacturer's protocols (10x Genomics; CG000338). Briefly, freshly prepared single-nuclei suspensions were counted on a Countess 3 FL cell counter and approximately 10,000 nuclei per condition went through 1hr of transposition at 37 °C followed by GEM generation and barcoding on a Chromium X machine with immediate subsequent reverse transcriptase reaction. cDNA was generated from 7 preAmp cycles and 8 cDNA cycles. GEX libraries were generated from fragmented cDNA and 14 SI cycles. ATAC libraries were generated from 7 preAmp cycles and 8 ATAC SI cycles. Library sequencing was performed on a NovaSeq 6000 S4 with 300 cycle Illumina flow cells by Novogene. Sequencing was demultiplexed and delivered as raw FASTQ files which were subsequently aligned using Cell Ranger Arc (cellranger-arc-2.0.2) to 10X Genomic's prebuilt GRCh38 reference genome using USC's HPC cluster.

Data, Materials, and Software Availability. RNA sequencing data have been deposited in GEO (GSE274904) (55). Previously published data were used for this work. [*SI Appendix*, Fig. S1*A* uses data published in Cell Metabolism in 2024 (17). *SI Appendix*, Fig. S2*B* uses data published in PNAS in 2017 (16). Fig. 1*A* and *SI Appendix*, Fig. S2*A* use data published in Developmental Cell in 2019 (12). Plasmids used were from data published in 2011 in Cell (56) and 2016 in PLoS ONE (57).]

ACKNOWLEDGMENTS. We thank all members of the McMahon lab, Drs. Nils O. Lindström, Francesca Mariani, and Nuria Pastor-Soler for their helpful discussions. We thank Nancy Wu, Yuntao Wang, and the Genome Modification Facility at USC for their assistance with generation of the CRISPR/Cas9-generated lines for this study. We thank Dr. Brendan Grubbs and Matthew Thornton for human fetal kidney samples and Yujing Yang and Connor Fausto for help in sub-setting human single nuclear data files for GEO submission. We would also like to thank Seth Ruffins and the Optical Imaging Facility for imaging assistance, Amanda S. Meyer and Sunghyun Kim for computational support, and Toni Sinwell and Jen Doias at the Genome Access Technology Center at the McDonnell Genome Institute at Washington University in St. Louis for technical support for bulk sequencing. R.K.P. was supported by NIH/NIDDK F31DK130597 fellowship and an American Society of Nephrology Pre-Doctoral Fellowship. D.K.K. was supported by NIH T32 fellowship 2T32HD060549.

1. A. Roy, M. M. Al-Bataineh, N. M. Pastor-Soler, Collecting duct intercalated cell function and regulation. *Clin. J. Am. Soc. Nephrol.* **10**, 305–324 (2015), 10.2215/CJN.08880914.
2. A. Taguchi *et al.*, Redefining the in vivo origin of metanephric nephron progenitors enables generation of complex kidney structures from pluripotent stem cells. *Cell Stem Cell* **14**, 53–67 (2014), 10.1016/j.stem.2013.11.010.
3. W. E. Lombard, J. P. Kokko, H. R. Jacobson, Bicarbonate transport in cortical and outer medullary collecting tubules. *Am. J. Physiol Renal Fluid Electrolyte Physiol.* **13**, 289–289 (1983), 10.1152/ajprenal.1983.244.3.f289.
4. J. B. Stokes, C. C. Tisher, J. P. Kokko, Structural-functional heterogeneity along the rabbit collecting tubule. *Kidney Int.* **14**, 585–593 (1978), 10.1038/ki.1978.167.
5. J. Kim, Y. H. Kim, J. H. Cha, C. C. Tisher, K. M. Madsen, Intercalated cell subtypes in connecting tubule and cortical collecting duct of rat and mouse. *J. Am. Soc. Nephrol.* **10**, 1–12 (1999), 10.1681/asn.v1011.
6. I. E. Royaux *et al.*, Pendrin, encoded by the pendred syndrome gene, resides in the apical region of renal intercalated cells and mediates bicarbonate secretion. *Proc. Natl. Acad. Sci. U.S.A.* **98**, 4221–4226 (2001), 10.1073/pnas.071516798.
7. D. Brown, S. Hirsch, S. Gluck, Localization of a proton-pumping ATPase in rat kidney. *J. Clin. Invest.* **82**, 2114–2126 (1988), 10.1172/JCI113833.
8. P. Teng-umnuay, J. W. Verlander, W. Yuan, C. C. Tisher, K. M. Madsen, Identification of distinct subpopulations of intercalated cells in the mouse collecting duct. *J. Am. Soc. Nephrol.* **7**, 260–274 (1996), 10.1681/asn.v72260.
9. V. L. Schuster, G. Fejes-Toth, A. Naray-Fejes-Toth, S. Gluck, Colocalization of H^+-ATPase and band 3 anion exchanger in rabbit collecting duct intercalated cells. *Am. J. Physiol. Renal Fluid Electrolyte Physiol.* **260**, 506–506 (1991), 10.1152/ajprenal.1991.260.4.f506.
10. Y. H. Kim *et al.*, Immunocytochemical localization of pendrin in intercalated cell subtypes in rat and mouse kidney. *Am. J. Physiol. Renal Physiol.* **283**, 744–754 (2002), 10.1152/ajprenal.00037.2002.
11. M. Soleimani *et al.*, Pendrin: An apical $Cl^-/OH^-/HCO_3^-$ exchanger in the kidney cortex. *Am. J. Physiol. Renal Physiol.* **280**, 356–364 (2001), 10.1152/ajprenal.2001.280.2.f356.
12. A. Ransick *et al.*, Single-cell profiling reveals sex, lineage, and regional diversity in the mouse kidney. *Dev. Cell* **51**, 399–413.e7 (2019), 10.1016/j.devcel.2019.10.005.
13. S. R. Blomqvist *et al.*, Distal renal tubular acidosis in mice that lack the forkhead transcription factor Foxi1. *J. Clin. Invest.* **113**, 1560–1570 (2004), 10.1172/JCI20665.
14. P. A. Stehberger *et al.*, Distal renal tubular acidosis in mice lacking the AE1 (Band3) Cl^-/HCO_3^- exchanger (slc4a1). *J. Am. Soc. Nephrol.* **18**, 1408–1418 (2007), 10.1681/ASN.2006101072.
15. X. Gao *et al.*, Deletion of hensin/DMBT1 blocks conversion of β- to α-intercalated cells and induces distal renal tubular acidosis. *Proc. Natl. Acad. Sci. U.S.A.* 109, 18625–18625 (2012), 10.1073/pnas.1217165109.
16. L. Chen *et al.*, Transcriptomes of major renal collecting duct cell types in mouse identified by single-cell RNA-seq. *Proc. Natl. Acad. Sci. U.S.A.* **114**, E9989–E9998 (2017), 10.1073/pnas.1710964114.
17. H. Li *et al.*, Transcriptomic, epigenomic, and spatial metabolomic cell profiling redefines regional human kidney anatomy. *Cell Metab.* **36**, 1105–1125.e10 (2024), 10.1016/j.cmet.2024.02.015.
18. V. S. Tanphaichitr *et al.*, Novel AE1 mutations in recessive distal renal tubular acidosis. Loss- of-function is rescued by glycophorin A. *J. Clin. Invest.* **102**, 2173–2179 (1998), 10.1172/JCI4836.
19. F. E. Karet *et al.*, Mutations in the chloride-bicarbonate exchanger gene AE1 cause autosomal dominant but not autosomal recessive distal renal tubular acidosis. *Proc. Natl. Acad. Sci. U.S.A.* **95**, 6337–6342 (1998), 10.1073/pnas.95.11.6337.
20. L. J. Bruce *et al.*, Familial distal renal tubular acidosis is associated with mutations in the red cell anion exchanger (band 3, AE1) gene. *J. Clin. Invest.* **100**, 1693–1707 (1997), 10.1172/JCI119694.
21. V. Pendred, Deaf-mutism and goitre. *Lancet* **148**, 532–532 (1896), 10.1016/S0140-6736(01)74403-0.
22. V. C. Sheffield *et al.*, Pendred syndrome maps to chromosome 7q21-34 and is caused by an intrinsic defect in thyroid iodine organification. *Nat. Genet.* **12**, 424–426 (1996), 10.1038/ng0496-424.
23. L. A. Everett *et al.*, Pendred syndrome is caused by mutations in a putative sulphate transporter gene (PDS). *Nat. Genet.* **17**, 411–422 (1997), 10.1038/ng1297-411.
24. N. Kandasamy, L. Fugazzola, M. Evans, K. Chatterjee, F. Karet, Life-threatening metabolic alkalosis in Pendred syndrome. *Eur. J. Endocrinol.* **165**, 167–170 (2011), 10.1530/EJE-11-0101.
25. I. Pela, M. Bigozzi, B. Bianchi, Profound hypokalemia and hypochloremic metabolic alkalosis during thiazide therapy in a child with Pendred syndrome. *Clin. Nephrol.* **69**, 450–453 (2008), 10.5414/CNP69450.
26. S. T. Wu *et al.*, Foxp1 is required for renal intercalated cell differentiation and acid-base regulation. *J. Am. Soc. Nephrol.* **35**, 533–548 (2024), 10.1681/ASN.0000000000000319.
27. M. Mukherjee, J. DeRiso, M. Janga, E. Fogarty, K. Surendran, Foxi1 inactivation rescues loss of principal cell fate selection in Hes1-deficient kidneys but does not ensure maintenance of principal cell gene expression. *Dev. Biol.* **466**, 1–11 (2020), 10.1016/j.ydbio.2020.08.005.
28. H. Jeong *et al.*, Inactivation of Notch signaling in the renal collecting duct causes nephrogenic diabetes insipidus in mice. *J. Clin. Invest.* **119**, 3290–3290 (2009), 10.1172/JCI38416.3290.
29. M. Mukherjee *et al.*, Endogenous notch signaling in adult kidneys maintains segment-specific epithelial cell types of the distal tubules and collecting ducts to ensure water homeostasis. *J. Am. Soc. Nephrol.* **30**, 110–126 (2019), 10.1681/ASN.2018040440.
30. Q. Guo *et al.*, Adam10 mediates the choice between principal cells and intercalated cells in the kidney. *J. Am. Soc. Nephrol.* **26**, 149–159 (2015), 10.1681/ASN.2013070764.
31. S. Kim *et al.*, Comparative single-cell analyses identify shared and divergent features of human and mouse kidney development. *Dev. Cell* **59**, 2912–2930.e7 (2024), 10.1016/j.devcel.2024.07.013.
32. R. K. Parvez *et al.*, Developmental and cell fate analyses support a postnatal origin for the cortical collecting system in the mouse kidney. *J. Am. Soc. Nephrol.*, 10.1681/ASN.0000000579 (2024).
33. H. K. Song *et al.*, Origin and fate of pendrin-positive intercalated cells in developing mouse kidney. *J. Am. Soc. Nephrol.* **18**, 2672–2682 (2007), 10.1681/asn.2006101076.
34. W. Wang, E. K. Chan, S. Baron, T. Van De Water, T. Lufkin, Hmx2 homeobox gene control of murine vestibular morphogenesis. *Development* 128, 5017–5029 (2001).
35. W. Wang *et al.*, Hmx2 and Hmx3 homeobox genes direct development of the murine inner ear and hypothalamus and can be functionally replaced by Drosophila Hmx. *Dev. Cell* **7**, 439–453 (2004).
36. W. Wang, T. Van De Water, T. Lufkin, Inner ear and maternal reproductive defects in mice lacking the Hmx3 homeobox gene. *Development* **125**, 621–634 (1998), 10.1242/dev.125.4.621.
37. Z. Zeng *et al.*, Generation of patterned kidney organoids that recapitulate the adult kidney collecting duct system from expandable ureteric bud progenitors. *Nat. Commun.* **12**, 1–15 (2021), 10.1038/s41467-021-23911-5.
38. M. Shi *et al.*, Human ureteric bud organoids recapitulate branching morphogenesis and differentiate into functional collecting duct cell types. *Nat. Biotechnol.* **41**, 252–261 (2023), 10.1038/s41587-022-01429-5.
39. M. Werth *et al.*, Transcription factor TFCP2l1 patterns cells in the mouse kidney collecting ducts. *eLife* **6**, e24265 (2017), 10.7554/eLife.24265.
40. H. Vidarsson *et al.*, The forkhead transcription factor Foxi1 is a master regulator of vacuolar H^+-ATPase proton pump subunits in the inner ear, kidney and epididymis. *PLoS ONE* **4**, e4471 (2009), 10.1371/journal.pone.0004471.
41. Y. Nishi *et al.*, A direct fate exclusion mechanism by Sonic hedgehog-regulated transcriptional repressors. *Development* **142**, 3286–3293 (2015), 10.1242/dev.124636.
42. H. Miyakawa, S. K. Woo, S. C. Dahl, J. S. Handler, H. M. Kwon, Tonicity-responsive enhancer binding protein, a Rel-like protein that stimulates transcription in response to hypertonicity. *Proc. Natl. Acad. Sci. U.S.A.* **96**, 2538–2542 (1999), 10.1073/pnas.96.5.2538.
43. M. Ono *et al.*, Characterization of gene expression in the kidney of renal tubular cell-specific NFAT5 knockout mice. *Am. J. Physiol. Renal Physiol.* **326**, F394–F410 (2023), 10.1152/ajprenal.00233.2023.
44. Q. Al-Awqati, Cell biology of the intercalated cell in the kidney. *FEBS Lett.* **587**, 1911–1914 (2013), 10.1016/j.febslet.2013.05.007.
45. J. van Adelsberg, J. C. Edwards, J. Takito, B. Kiss, Q. Al-Awqati, An induced extracellular matrix protein reverses the polarity of band 3 in intercalated epithelial cells. *Cell* **76**, 1053–1061 (1994), 10.1016/0092-8674(94)90382-4.
46. A. J. Modzelewski *et al.*, Efficient mouse genome engineering by CRISPR-EZ technology. *Nat. Protoc.* **13**, 1253–1274 (2018), 10.1038/nprot.2018.012.
47. E. Zuo *et al.*, One-step generation of complete gene knockout mice and monkeys by CRISPR/Cas9-mediated gene editing with multiple sgRNAs. *Cell Res.* **27**, 933–945 (2017), 10.1038/cr.2017.81.
48. M. W. Davis, E. M. Jorgensen, ApE, a plasmid editor: A freely available DNA manipulation and visualization program. *Front. Bioinf.* **2**, 1–15 (2022), 10.3389/fbinf.2022.818619.
49. R. K. Parvez, A. P. McMahon, Dmrt2 and Hmx2 direct intercalated cell diversity in the mammalian kidney through antagonistic and supporting regulatory processes. Gene Expression Omnibus. https://www.ncbi.nlm.nih.gov/geo/query/acc.cgi?acc=GSE295893. Deposited 29 April 2025.
50. X. Qiu *et al.*, Single-cell mRNA quantification and differential analysis with census. *Nat. Methods* **14**, 309–315 (2017), 10.1038/nmeth.4150.
51. X. Qiu *et al.*, Reversed graph embedding resolves complex single-cell trajectories. *Nat. Methods* **14**, 979–982 (2017), 10.1038/nmeth.4402.
52. C. Trapnell *et al.*, The dynamics and regulators of cell fate decisions are revealed by pseudotemporal ordering of single cells. *Nat. Biotechnol.* **32**, 381–386 (2014), 10.1038/nbt.2859.
53. L. Xiong *et al.*, Direct androgen receptor control of sexually dimorphic gene expression in the mammalian kidney. *Dev. Cell* **58**, 2338–2358.e5 (2023), 10.1016/j.devcel.2023.08.010.
54. Y. Shi *et al.*, Haploinsufficiency leads to neurodegeneration in C9ORF72 ALS/FTD human induced motor neurons. *Nat. Med.* **24**, 313–325 (2018), 10.1038/nm.4490.
55. R. K. Parvez, A. P. McMahon, Dmrt2 and Hmx2 direct intercalated cell diversity in the mammalian kidney through antagonistic and supporting regulatory processes. Gene Expression Omnibus. https://www.ncbi.nlm.nih.gov/geo/query/acc.cgi?acc=GSE274904. Deposited 15 August 2025.
56. M. Gabut *et al.*, An alternative splicing switch regulates embryonic stem cell pluripotency and reprogramming. *Cell* **147**, 132–146 (2011), 10.1016/j.cell.2011.08.023.
57. A. P. Adam, A. M. Lowery, N. Martino, H. Alsaffar, P. A. Vincent, Src family kinases modulate the loss of endothelial barrier function in response to TNF-α: Crosstalk with p38 signaling. *PLoS ONE* **11**, 1–20 (2016), 10.1371/journal.pone.0161975.